Journal Name

ARTICLE TYPE

Cite this: DOI: 10.1039/xxxxxxxxxx

Bayesian determination of the effect of a deep eutectic solvent on the structure of lipid monolayers

Andrew R. McCluskey,[ab‡] Adrian Sanchez-Fernandez,[ac‡¶] Karen J. Edler,[a*] Stephen C. Parker,[a] Andrew J. Jackson,[cd] Richard A. Campbell,[ef] and Thomas Arnold[abcg*]

Received Date
Accepted Date

DOI: 10.1039/xxxxxxxxxx

www.rsc.org/journalname

Deep eutectic solvents present a novel class of non-aqueous room temperature solvent with tunable properties, that are capable of promoting the self-assembly of surfactant molecules. However, the solvation model in these systems still challenges the classic understanding of amphiphilicity. In this work, we present the first example of the self-assembly of phospholipid monolayers at the interface between air and a non-aqueous solvent. Furthermore, we use novel, chemically-consistant Bayesian modelling of X-ray and neutron reflectometry measurements to show the ability of the deep eutectic solvent to interact with the phosphatidylglycerol lipid head component, leading to an apparent increase in the component volume compared to that observed in water. No such change was observed for the phosphocholine head component, indicating that the interaction is head component specific.

Introduction

Deep eutectic solvents (DES) are green, sustainable solvents obtained through the complexation of naturally occurring compounds, such as sugars, alcohols, amines and carboxylic acids, among others.[1,2] An extensive hydrogen-bonding network is present between these precursors, allowing the mixture to remain liquid at room temperature.[3–5] Additionally, through different combinations of the precursor materials, it is possible to tune the physicochemical properties of the solvent, such as polarity,[6] viscosity and surface tension,[1] network charge,[7] and hydrophobicity.[8,9]

It has recently been shown that these solvents have the ability to promote the self-assembly of surfactants into micellar structures[10,11] and to stabilise the conformation of non-ionic polymer species,[12] indicating the presense of a solvophobic effect. The behaviour and conformation of biomolecules in DES have seen an increase in interest,[13–20] due to the potential application of DES as environments for enzymatic reactions.[21] Futhermore, recent investigations have also shown that DES are able to support the formation of phospholipid bilayers.[22–24]

The formation of phospholipid monolayers at the air/liquid interface plays a key role in many biological and technological processes. The solvent-specific solubility of different components of the phospholipid results in the formation of a stable monolayer of phospholipid at the interface.[25] Phospholipids contain a charged head, either anionic or zwitterionic, and investigations at the air-salt water interface have revealed the importance of the phospholipid-ion interactions on structure, monomer packing, and stability of the monolayer.[25,26] Despite the broad interest in these systems, the presence of stable phospholipid monolayers at the interface between air and a non-aqueous media has not been previously reported, to the best of the authors' knowledge.

Recent developments in computational resources and software have enabled powerful methodologies and algorithms to be harnessed by those from non-expert backgrounds. This has benefitted significantly from open-source software projects such as the Python language[27] and the Jupyter notebooks framework.[28] In the area of neutron and X-ray reflectometry data-analysis, the landscape of open-source software is diverse, with a range of software packages available from a variety of sources; refnx[29], motofit,[30] Aurore,[31] and GenX.[32] The Python library refnx is particularly powerful due to the ability to implement complete custom models which can contain chemically-relevant information.

[a] Department of Chemistry, University of Bath, Claverton Down, Bath, BA2 7AY, UK.
[b] Diamond Light Source, Harwell Campus, Didcot, OX11 0DE, UK.
[c] European Spallation Source, SE-211 00 Lund, Sweden.
[d] Department of Physical Chemistry, Lund University, SE-211 00 Lund, Sweden.
[e] Institut Laue-Langevin, 71 avenue des Martyrs, 38000, Grenoble, France.
[f] Division of Pharmacy and Optometry, University of Manchester, Manchester, M13 9PT, UK.
[g] ISIS Neutron and Muon Source, Science and Technology Facilities Council, Rutherford Appleton Laboratory, Harwell Oxford, Didcot OX11 0QX, UK.
¶ Present address: Department of Food Technology, Lund University, SE-211 00 Lund, Sweden
* Corresponding author: k.edler@bath.ac.uk, tom.arnold@esss.se
† Electronic Supplementary Information (ESI) available: All datasets, figure file and analysis/plotting scripts, allowing for a fully reproducible analysis of all work presented herein. See DOI: 10.6084/m9.figshare.6661784
‡ These authors have contributed equally to the work presented within.

The use of a Python library for fitting enables powerful probability distribution function (PDF) sampling methods to be used such as the Goodman & Weare Affine Invariant Markov chain Monte Carlo (MCMC) Ensemble,[33] as implemented in the Python library emcee.[34] This is a method for sampling a high-dimensionality parameter space, such as that which is relevant in reflectometry fitting, in a Bayesian fashion, where the new samples are generated with consideration of those sampled previously. The use of Bayesian inference allows the PDF for each fitting variable to be probed, therefore estimations of the inverse uncertainties associated with each parameter can be found, as well as information about the correlations between different variables.

In this work, we present the first investigation of the structure of phospholipid monolayers at the air-DES interface, as determined by chemically-consistant modelling of X-ray reflectometry (XRR) measurements. Four different phospholipids; 1,2-dipalmitoyl-sn-glycero-3-phosphocholine (DPPC), 1,2-dimyristoyl-sn-glycero-3-phosphocholine (DMPC), 1,2-dilauroyl-sn-glycero-3-phosphocholine (DLPC) and 1,2-dimyristoyl-sn-glycero-3-phospho-(1'-rac-glycerol) (DMPG), were studied at the interface between a 1:2 mixture of choline chloride:glycerol and air. This allowed the nature of two, chemically distinct, phospholipid head components to be understood in this non-aqueous solvent, in addition to the effect of the tail chain length. The analysis was then extended to model complementary neutron reflectometry measurements for two contrasts of DMPC and DPPC at a single surface pressure.

Experimental

Materials

Choline chloride (99 %, Sigma-Aldrich) and glycerol (99 %, Sigma-Aldrich) d_9-choline chloride (99 %, 98 % D, CK Isotopes) and d_8-glycerol (99 %, 98 % D, CK Isotopes) were purchased and used without further purification. The DES was prepared by mixing the precursors at the appropriate ratio, and heating at 80 °C until a homogeneous, transparent liquid formed.[1] The solvent was equilibrated overnight at 40 °C and subsequently stored under a dry atmosphere. Due to the limited availability of the deuterated precursors, a fully protonated subphase (hDES) and a partially deuterated subphase (hdDES) were prepared and used during the neutron reflectometry (NR) experiment. The partially deuterated subphase was prepared using the following mixtures of precursors: 1 mole of 0.38 fraction of h-choline chloride/0.62 mole fraction of d-choline chloride; and 2 moles of 0.56 mole fraction of h-glycerol/0.44 mole fraction of d-glycerol. The solvent was subsequently prepared following the procedure discussed above.

The water content of the DES was determined before and after each experiment by Karl-Fischer titration (Mettler Toledo DL32 Karl-Fischer Coulometer, Aqualine Electrolyte A, Aqualine Catholyte CG A) in order to ensure water presence was kept to a minimum. Those measurements showed that the water content of the solvent was kept below 0.3 wt% during all the experimental procedures presented here, which we assume to be negligible and have to little impact on the characteristics of the DES.[3,4]

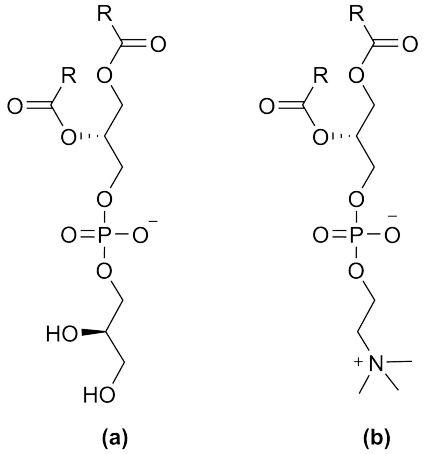

Fig. 1 The two lipid classes with different head components compared in this study, where R indicates the hydrocarbon tail; (a) phosphatidylglycerol, (b) phosphocholine.

DPPC (> 99 %, C_{16} tails), DMPC (> 99 %, C_{14} tails), and DMPG (> 99 %, C_{14} tails) were supplied by Avanti Polar Lipids and DLPC (> 99 %, C_{12} tails) was supplied by Sigma-Aldrich and all were used as received. Deuterated versions of DPPC (d_{62}-DPPC, > 99 %, deuterated tails-only) and DMPC (d_{54}-DPPC, > 99 %, deuterated tails-only) were supplied by Avanti Polar Lipids and used without further purification. These phospholipids were dissolved in chloroform (0.5 mg/mL) at room temperature. PC indicates the molcule contains a phosphocholine head component, where PG contains a phosphatidylglycerol head component, these are shown in Figure 1.

In the XRR experiment, sample preparation was performed in situ using the standard method for the spreading of insoluble monolayers on water: a certain amount of the phospholipid solution was spread onto the liquid surface in order to provide a given surface concentration. After the evaporation of the chloroform, it is assumed that the resulting system is a solvent subphase with a monolayer of phospholipid at the interface. Surface concentration was modified by closing and opening the PTFE barriers of a Langmuir trough. In order to minimise the volumes used in the NR experiment (to keep the cost of deuterated compounds to a manageable level) it was not possible to use a Langmuir trough. Instead, small Delrin adsorption troughs were used that did not have controllable barriers. So, although the surface coverage was nominally the same as used in the X-ray studies, the lack of precise control over the surface pressure meant that it was not appropriate to co-refine XRR and NR contrasts together.

Methods

XRR measurements were taken on I07 at Diamond Light Source, at 12.5 keV photon energy using the double-crystal-deflector.[41] The reflected intensity was measured in a momentum transfer range from 0.018 to 0.7 $Å^{-1}$. The data were normalised with respect to the incident beam and the background was measured from off-specular reflection and subsequently subtracted. Samples were equilibrated for at least one hour and preserved under

Table 1 Lipid component volumes extracted from different literature sources. V_l corresponds to the total lipid volume, MD to molecular dynamics simulation, WAXS to wide-angle X-ray scattering, NB to neutral buoyancy and DVTD to differential vibrating tube densimetry. [a] The values for the head component in Kucerka *et al.*,[35] were taken from Balgavý *et al.*[36]

Lipid	DPPC			DMPC		DLPC		DMPG	POPG
Reference	[37]	[38]	[35, 36][a]	[37]	[35, 36][a]	[37]	[35, 36][a]	[39]	[40]
V_l/Å^3	1287.3 ± 25.5	1148 ± 2	1264.2 ± 32.1	1172.5 ± 25.1	1155.4 ± 30.0	1057.7 ± 24.7	1046.6 ± 28.0	1011.4	1203
V_t/Å^3	966.4 ± 5.4	829 ± 4	924.7 ± 17.6	851.5 ± 5.0	815.9 ± 15.5	736.8 ± 4.6	707.1 ± 13.5	720.4	914
V_h/Å^3	320.9 ± 20.1	319 ± 6	339.5 ± 14.5	320.9 ± 20.1	339.5 ± 14.5	320.9 ± 20.1	339.5 ± 14.5	291.0	289
Method	MD	WAXS	NB	MD	NB	MD	NB	DVTD	MD
T/°C	50	24	30	50	30	50	30	20	25

an argon atmosphere to minimise the adsorption of water by the subphase. XRR data were collected for each of the lipids, DLPC, DMPC, DPPC and DMPG at four surface pressures (DLPC: 20, 25, 30, and 35 mNm^{-1}, DMPC: 20, 25, 30, and 40 mNm^{-1}, DPPC: 15, 20, 25, and 30 mNm^{-1}, DMPG: 15, 20, 25, and 30 mNm^{-1}), as measured with an aluminium Wilhelmy plate; all measurements were conducted at 22 °C. The aluminium Wilhelmy plate was used over a traditional paper plate due to the low wetability of paper by the DES.

The NR experiments were performed on FIGARO at the Institut Laue-Langevin using the time-of-flight method.[42] Data at two incident angles of 0.62° and 3.8° were measured to provide a momentum transfer range from 0.005 to 0.18 Å^{-1}. Two surface pressures for each system and contrast was measured (DMPC: 20 and 25 mNm^{-1}, DPPC: 15 and 20 mNm^{-1}). Similar to the X-ray procedure, samples were given enough time to equilibrate (at least two hours), kept under an inert atmosphere, and all measurements were conducted at 22 °C.

Data analysis

The use of XRR and NR to analyse the structure of phospholipids on the surface of water has a history extending over many years.[25,26,43–47] The models used in the rationalisation of XRR and NR data have varied significantly in number of layers present, use of interfacial roughness, and parameterisation of physical constraints. Frequently these physical constraints include the component volumes of the phospholipid head and tail components, using values taken from other techniques, such as those shown in Table 1. Additionally, a recent evaluation of the applicability of different models to surfactant and phospholipid monolayers from the NR perspective has been published,[48] that suggests possible oversights in the modelling of NR data.

In Table 1, there appears to be a general consensus that the component volume of the phosphocholine (PC) head is in the range from 320-360 Å^3 while the phosphatidylglycerol (PG) head is in the range 289-291 Å^3. However, we do not know whether the head component volumes used in the literature, that are derived from water-based measurements, will be appropriate for this work, which involves a non-aqueous solvent. The charged nature of the zwitterionic and anionic lipid heads means that they are likely to have different interactions with polar, but neutral, water as compared to the charged DES components.[49] Furthermore, it has been shown that in the liquid expanded and condensed phases, which are often present at high surface pressure, the lipid tails will become compressed resulting in a component volume less than measured from other techniques,[50,51] and the need to take into account the compaction of the hydrocarbon chains of phospholipid monolayers according to their phase in the modelling of NR data has recently been demonstrated.[48]

In this work we would therefore like to use a model that does not assume the molecular volume while remaining physical meaningful. To do this we have allowed the lipid component volumes to vary while constraining the overall system to be self-consistent across multiple different measurements. To do this we have used the Python library refnx[29]. This software allows the inclusion of a custom model to be defined, from which parameters feed into the Abelès reflectivity model (a model that is widely used to calculate reflectivity[52,53]). This custom model, along with a series of Jupyter notebooks showing, in full, the analysis performed, can be found in the ESI and is available under CC-BY.[54]

Our chemically-consistent model is made up of two layers to define the lipid monolayer; the head layer at the interface with the solvent and tail layer at the interface with the air. The head components have a calculated scattering length, b_h, (found as a summation of the X-ray or neutron atomic scattering lengths), and a component volume, V_h. These head components make up a layer with a given thickness, d_h, and roughness, σ_h, within which some volume fraction of solvent can intercalate, ϕ_h. The tail components also have a calculated scattering length, b_t, roughness, σ_t, and a component volume, V_t. We have defined the thickness of the tail layer, d_t, in terms of the maximum (all-trans) length of the carbon tail, t_t, and the angle that the chain is tilted by with respect to the interface normal, θ_t,

$$d_t = t_t \cos\theta_t. \tag{1}$$

This was used to impose a chemically-sensible maximum on the thickness of the lipid tail layer, e.g. it cannot be thicker than the maximum extended length of the lipid tail. The scattering length density (SLD) of the tail and head layers used in the Abelès model can therefore be found as follows,

$$\mathrm{SLD}_i = \frac{b_i}{V_i}(1-\phi_i) + \mathrm{SLD}_s(\phi_i), \tag{2}$$

where, SLD_s is the scattering length density of the subphase (DES), and i indicates either the tail or head layer; it is assumed that the tail layer contains neither solvent nor air, e.g. $\phi_t = 0$. To ensure that the number density of head components and pairs of tail components is the same, the following constraint was in-

cluded in the model,[55]

$$\phi_h = 1 - \left(\frac{d_t V_h}{V_t d_h}\right). \quad (3)$$

Based on the work of Campbell *et al.*,[48] a single value for the interfacial roughness was fitted for all of the interfaces, including the subphase (i.e. $\sigma_h = \sigma_t = \sigma_s$), as there is only a single lipid molecule type in each monolayer. Therefore, any capillary wave roughness at the air-DES interface is carried equally through the layers.

In the first of two steps, this custom model was used to co-refine the component volume of the lipid head component, V_h, the volume of the tail component, V_t, and the head thickness, d_h across XRR measurements at four different surface concentrations. In keeping with the work of Campbell *et al.*,[48] a single value for the head thickness was fitted for each lipid across all surface pressures, as the thickness of the head layer was considered to be dependent on molecular dimensions only. The following parameters were allowed to vary; θ_t, and $\sigma_{t,h,s}$, independently across the surface pressures, while others, shown in Table 2, were held constant at the values given. The length of the carbon chain was kept constant at the value determined by the Tanford equation,[56] since this is the maximum chain length possible and the most likely conformation at the surface pressures studied.[57] For each co-refinement of four XRR measurements, there were, in total, eleven degrees of freedom in the fitting process. Throughout all of the analysis, the reflectometry scale factor was allowed to vary freely, while the background as constrained to the intensity of either the largest or second-largest q-value.

Table 2 The invariant parameters within the chemically-consistent model. [a]Values obtained from the Tanford formula.[56] [b]Values obtained from Sanchez-Fernandez *et al.*[10]

Component	b_t/fm	b_h/fm	t_t/Å	SLD/$\times 10^{-6}$Å^{-2}
X-ray				
DLPC	5073	4674	15.5[a]	–
DMPC	5985	4674	18.0[a]	–
DPPC	6897	4674	20.5[a]	–
DMPG	5985	4731	18.0[a]	–
Air	–	–	–	0
DES	–	–	–	10.8[b]
Neutron				
d_{54}-DMPC	5329.8	602.7	18.0[a]	–
d_{62}-DPPC	6129.2	602.7	20.5[a]	–
h-DES	–	–	–	0.43[b]
hd-DES	–	–	–	3.15[b]

In the second step, the head and tail component volumes, and head layer thickness determined from XRR were fixed for the refinement of the custom model against the NR measurements. This approach means that the number of variable parameters to fit the NR data can be reduced to two, namely the chain tilt angle, θ_t, and the interfacial roughness, $\sigma_{t,h,s}$, for the co-refinement of two datasets. Table 2 also gives the details of the scattering lengths and SLDs used as invariant parameters for the NR fitting.

In both cases, the refinement of the custom model to the experimental data involved the transformation of the reflectometry calculated from the model and the data into Rq^4 such that the

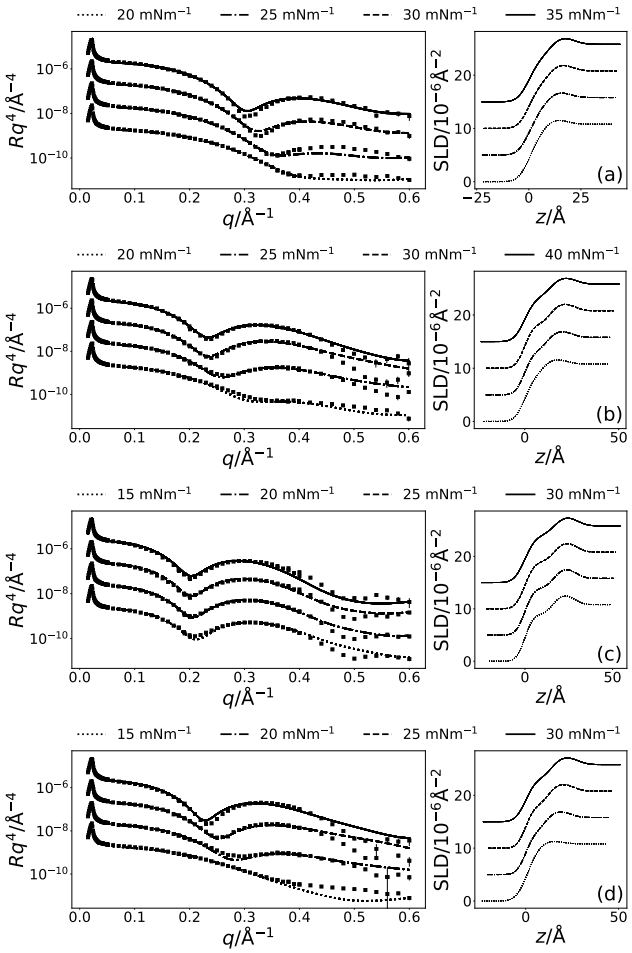

Fig. 2 The XRR profiles (left) and SLD profiles (right) for each of the four lipids; (a) DLPC, (b) DMPC, (c) DPPC, (d) DMPG, at the four measured surface pressures; 15, 20, 25, 30, 35, 40 mNm^{-1} (coloured blue, yellow, green, orange, pink, and brown respectively). The different surface pressure XRR profiles have been offset in the y-axis by an order of magnitude and SLD profiles offset in the y-axis by 5×10^{-6} Å^{-2}, for clarity.

contribution of the Fresnel decay was removed, before using the differential evoluation method available to refnx from the scipy library,[58] to find the parameters that gave the best fit to the data. The parameter space was then probed using the MCMC method available through emcee,[34] which allowed for an estimate of the probability distribution function (PDF) associated with each parameter. In the MCMC sampling, 200 walkers were used over 1000 iterations, following an equilibration of 200 iterations. The use of MCMC sampling allowed for the Bayesian inference of the PDF for each of the variables and their respective interactions (shown in detail in the ESI). This allowed asymmetric confidence intervals to be found for each of the variable parameters. However, it is important to note that these are not *true* confidence intervals, and account only for the uncertainty present in the data, i.e. they do no account of systematic uncertainty in the measurement that are underrepresented, or unrepresented, in the experimental dataset.

Table 3 The best-fit values, and associated 95 % confidence intervals for the varying parameters in the XRR models, at the highest surface pressure (SP) measured. The values of d_t were found from the values of θ_t using Eqn. 1 and the values for ϕ_h were obtained from the use of Eqn. 3

Lipid	DLPC	DMPC	DPPC	DMPG
SP/mNm^{-1}	35	40	30	30
θ_t/°	$48.18^{+0.22}_{-0.22}$	$39.78^{+0.07}_{-0.06}$	$34.47^{+0.07}_{-0.07}$	$38.92^{+0.06}_{-0.06}$
$\sigma_{t,h,s}$/Å	$4.35^{+0.03}_{-0.02}$	$4.53^{+0.01}_{-0.01}$	$4.90^{+0.00}_{-0.00}$	$4.44^{+0.01}_{-0.01}$
V_t/Å^3	$625.21^{+3.70}_{-4.06}$	$718.75^{+0.55}_{-0.53}$	$765.32^{+0.40}_{-0.37}$	$733.99^{+0.60}_{-0.60}$
V_h/Å^3	$331.43^{+0.64}_{-0.64}$	$339.55^{+0.29}_{-0.28}$	$322.00^{+0.24}_{-0.25}$	$329.94^{+0.34}_{-0.33}$
d_h/Å	$10.99^{+0.13}_{-0.14}$	$13.21^{+0.04}_{-0.04}$	$12.70^{+0.03}_{-0.03}$	$13.95^{+0.03}_{-0.03}$
$\phi_h/\times10^{-2}$	$50.31^{+1.17}_{-1.22}$	$50.57^{+0.24}_{-0.23}$	$43.96^{+0.23}_{-0.22}$	$54.91^{+0.19}_{-0.19}$
d_t/Å	$10.30^{+0.05}_{-0.04}$	$13.82^{+0.01}_{-0.01}$	$16.91^{+0.01}_{-0.01}$	$13.99^{+0.01}_{-0.01}$

Results & Discussion

The chemically-consistent model was co-refined across the four surface pressure XRR measurements for each lipid. The resulting XRR profiles and associated SLD profiles are shown in Figure 2. Table 3 gives details of all varied parameters for each lipid at the highest surface pressure measured, as well as the details of d_t and ϕ_h which are determined from Eqns. 1 and 3 respectively. Each value is given with asymmetric uncertainies that corresponds to a 95 % confidence interval of the PDF; the full PDF plots can be found in the ESI.

The custom model was used to co-refine the two contrasts of NR measurements for each lipid, at each surface pressure. The resulting NR profiles and associated SLD profiles, at a surface pressure of 20 mNm^{-1} are given in Figure 4. Table 4 gives details of the varied parameters at each surface pressure as well as d_t and ϕ_h, again determined from Eqns. 1 and 3. These are, once again, given with a asymmetric uncertainties corresponding to a 95 % confidence interval and the full PDF plots can be found in the ESI.

Effect of compression on monolayer thickness

Table 3 gives the best-fit values for each lipid at the highest surface pressure measured. From this, we can see that, as expected and as found in previous work,[25,59] the thickness of the tail layer increases as the number of carbon atoms in the tail chain increases. Furthermore, the thickness of the tail layers in these monolayers appears to agree well with values found for water-analogues; $13.72^{+0.01}_{-0.01}$ Å at 30 mN/m in DES compared with $d_t = 15.8$ Å at 30 mN/m[44] in water for DMPC, and $16.91^{+0.01}_{-0.01}$ Å at 30 mN/m in DES compared with $d_t = 16.7$ Å at 40 mN/m[46] in water for DPPC.

The variation of the tail layer thickness in the models with surface pressure is given for each lipid in Figure 3. It can be observed that as the surface pressure increases, the thickness of the tail layer increases to a point, before plateauing; for DPPC this occurs at 20 mNm^{-1}, DMPC at 30 mNm^{-1} and for DMPG and DLPC can be assumed to be at higher pressures than those studied. This phenomenon of the tail thickness increasing with increasing surface pressure has been noted before for DMPC[43] and DPPC[48] at the air-water interface.

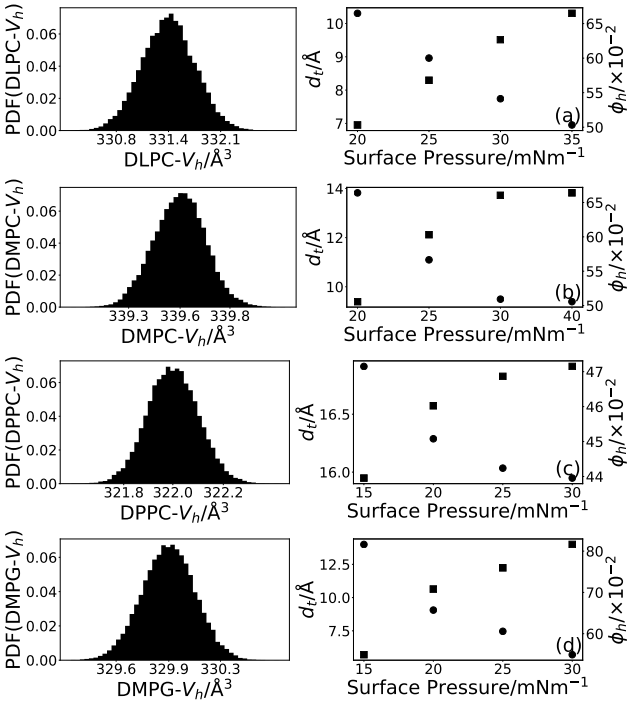

Fig. 3 The PDFs of the head component volume (left) and variation of d_t (blue squares) and ϕ_h (green circles) with surface pressure for each of the four lipids; (a) DLPC, (b) DMPC, (c) DPPC, (d) DMPG.

Effect of compression on solvent concentration

In Figure 3, it is clear that for all four lipids, as the surface pressure is increased there is a corresponding decrease in the percentage solvent present in the lipid head layer. This can be rationalised by considering that when the surface pressure is increased, the free volume available to the solvent between the lipid head components reduces forcing the solvent out of the lipid head layer and into the bulk. A similar effect has been observed when increasing the surface pressure from 11 mNm^{-1} to 31 mNm^{-1}) for a DMPC/DMPG monolayer at the air-water interface.[43]

Effect of compression on the lipid tail component volumes

It can be seen by comparing Tables 1 and 3 that the volume of the lipid tails are significantly lower in the current measurements than found previously, by other techniques. It is unlikely that this is a result of the DES subphase, due to the hydrophobic nature of the lipid tails. However, this reduction has been shown previously,[48] where it was rationalised by the compaction of the monolayer at elevated surface pressure. In that work, the optimal value of the tail component volume for DPPC was found to be 772 Å^3 at a surface pressure of 35 mNm^{-1}, this agrees well with the value of $765.32^{+0.40}_{-0.37}$ Å^3 found in this work at surface pressures of 15, 20, 25, and 30 mNm^{-1}.

In this work, a single tail component volume was fitted to each lipid for all four surface pressures that were measured. This is based on the assumption, that at all four surface pressures, the lipids adopt the same phase (as discussed in the ESI) and therefore any variation in the structure with surface pressure would manifest only as a change in the tail thickness, via the chain tilt

angle. It is clear when comparing Tables 1 and 3 that some of the tail component volumes are also reduced in the current XRR measurements compared to those determined previously. The reduction was found to be between 8-12 % for DPPC, DMPC and DLPC when compared with literature sources at 24-30 °C, this is in good agreement with the maximum compression percentage of 15 % noted by Small and coworkers.[51] DMPG shows a small increase in the tail volume relative to the literature value quoted at lower temperature. Notably this value is similar to that found in this work for DMPC, which has the same tail structure and suggests that our results are at least self-consistent.

Solvent effect on lipid head component volumes

Figure 3 shows the PDFs determined for the head component volume for each of the four lipids. The three lipids with the PC head component are consistent, giving values of ~ 330 Å^3, regardless of tail component. This agrees well with the values found for the same head component in water, shown in Table 1. Interestingly, the component volume for the PG head is similar to that for the PC head with a value of $329.94^{+0.34}_{-0.33}$ Å^3. The PG head component volume in water, from either DMPG using differential vibrating tube densimetry[39] or POPG using molecular dynamics simulations,[40] is noticeably smaller. This indicates that there may be some effect arising from the solvation in choline cloride:glycerol causing an apparent increase in the PG component volume when compared with water.

The major difference between the two head components is the fact PG component is negatively charged whereas the PC component is zwitterionic. It has been shown previously that the conformation for the PC component is folded in water,[60] due to the interaction between the positively-charged ammonium and the negatively-charged phosphate groups. A similar structure may occur for the PG component, with the interaction between the partially postively-charged alcoholic hydrogen atoms and the negatively-charged phosphate group. However, such an interaction would be weaker than that observed in the PC component. Therefore, this observed increase found for the PG component volume in DES when compared with water may be due to the unfolding of the PG head. This unfolding would be made possible by the charged nature of the solvent providing a greater screening effect for the PG head than are present in water. This effect may not be observed for the PC component due to the greater strength of the folding arising from the formally-charged nature of the ammonium group. It would be anticipated that this unfolding would result in an increase in the thickness of the lipid head layer. Previously, DPPG has been reported to have a head layer thickness of 10.3 ± 0.4 Å at 22 mNn^{-1} from neutron reflectometry measurements,[45] which it slightly less than the $13.95^{+0.03}_{-0.03}$ Å determined in the current work, further suggesting that the unfolding of the PG head component may be occurring as a result of interaction with the DES.

Refinement of neutron reflectometry

The ability to fit the NR data, as shown in Figure 4 indicates that the values found for the head component volume is consistant between the pair of measurements for the same system. It is clear, that again stable monolayers of the lipids are forming at the air-DES interface, and that the component volumes determined from XRR measurements are robust enough to be used in the modelling of NR data. Futhermore, the trends observed with increasing surface pressure in the XRR models, pertaining to the increasing tail thickness and decreasing solvent concentration in the head components are consistant with that found in the NR models.

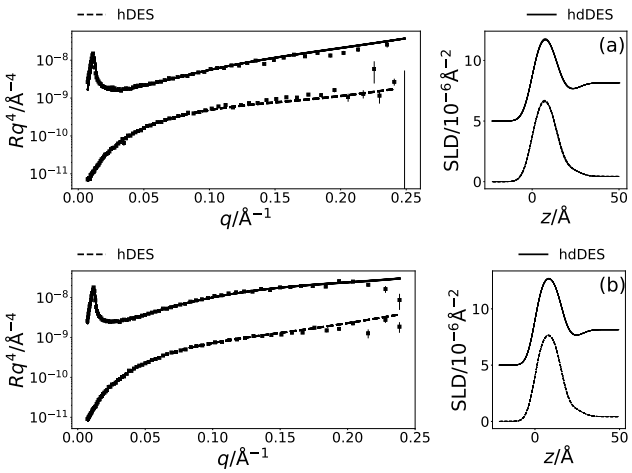

Fig. 4 The NR and SLD profiles at a surface pressure of 20 mNm^{-1}, the h-DES contrast is shown in blue while the hd-DES in green; (a) DMPC, (b) DPPC. The NR profiles have been offset in the y-axis by an order of magnitude and SLD profiles offset in the y-axis by 5×10^{-6} Å^{-2}, for clarity.

Table 4 The best-fit values, and associated 95 % confidence intervals for the varying parameters in the co-refined NR models. The values of d_t were found from the appropriate values of θ_t using Eqn. 1, and the values of ϕ_h were found using Eqn. 3.

Lipid	d_{54}-DMPC		d_{62}-DPPC	
SP/mNm^{-1}	20	25	15	20
θ_t/°	$38.98^{+0.75}_{-0.75}$	$24.65^{+0.06}_{-0.01}$	$53.11^{+0.45}_{-0.45}$	$40.67^{+0.42}_{-0.42}$
$\sigma_{t,h,s}$/Å	$4.41^{+0.16}_{-0.16}$	$2.51^{+0.03}_{-0.01}$	$4.27^{+0.16}_{-0.17}$	$3.98^{+0.10}_{-0.10}$
$\phi_h/\times 10^{-2}$	$50.00^{+0.52}_{-0.53}$	$41.54^{+0.01}_{-0.03}$	$59.20^{+0.43}_{-0.43}$	$48.45^{+0.32}_{-0.32}$
d_t/Å	$13.98^{+0.15}_{-0.15}$	$16.35^{+0.00}_{-0.01}$	$12.32^{+0.13}_{-0.13}$	$15.56^{+0.10}_{-0.10}$

Conclusions

For the first time, stable phosphocholine and phosphatidylglycerol lipid monolayers have been observed and characterised on a non-aqueous liquid surface. Until the emergence of ionic liquids and DES, only a limited number of molecular solvents exhibited the ability to promote self-assembly and, to the best of our knowledge, only water among those had demonstrated the formation of phospholipid monolayers at the air-liquid interface.

A physically and chemically constrained modelling approach and Bayesian analysis method was used to rationalise these measurements showing that the structures are remarkably similar at the air-DES interface to those previously observed at the air-water interface. This has the important implication that DES therefore offer the possibility of performing studies of model membranes in the absence of water. Such applications may include fundamental investigations of phospholipid monolayers in extreme en-

vironments (total or partial absence of water, cryogenic temperatures), protein membrane interactions and development of new technologies for drug delivery. However, the PG component did show a significant difference; having a larger head component volume than observed for the same system in water. This suggests that the transfer of lipids to a DES is not just a simple substitution of the subphase. In this specific case we have proposed an explanation based on unfolding of the PG head component that is enabled by electrostatic screening of the component charges by the partially charged solvent.

The ability to determine the head component volume was facilitated by access to easy to use, open-source software that allowed for the straightforward use of a custom, chemically-consistant model within the analysis of the XRR and NR measurements. Futhermore, this work presents the first, to our knowledge, use of chemically-consistant parameterisation to co-refine XRR measurements at different surface concentrations.

Conflicts of interest

There are no conflicts to declare.

Acknowledgements

The authors thank the European Spallation Source and the University of Bath Alumni Fund for supporting A.S.-F. A.R.M. is grateful to the University of Bath and Diamond Light Source for co-funding a studentship (Studentship Number STU0149). We also thank Diamond Light Source (Experiment Number: SI10546-1) and Institut Laue-Langevin (DOI: 10.5291/ILL-DATA.9-13-612) for the awarded beamtime.

Notes and references

1 E. L. Smith, A. P. Abbott and K. S. Ryder, *Chem. Rev.*, 2014, **114**, 11060–11082.

2 Y. Dai, J. van Spronsen, G. J. Witkamp, R. Verpoorte and Y. H. Choi, *Anal. Chim. Acta.*, 2013, **766**, 61–68.

3 O. S. Hammond, D. T. Bowron and K. J. Edler, *Green Chem.*, 2016, **18**, 2736–2744.

4 O. S. Hammond, D. T. Bowron, A. J. Jackson, T. Arnold, A. Sanchez-Fernandez, N. Tsapataris, V. G. Sakai and K. J. Edler, *J. Phys. Chem. B*, 2017, **121**, 7473–7483.

5 C. F. Araujo, J. A. P. Coutinho, M. M. Nolasco, S. F. Parker, P. J. A. Ribeiro-Claro, S. Rudic, B. I. G. Soares and P. D. Vaz, *Phys. Chem. Chem. Phys*, 2017, **19**, 17998–18009.

6 A. Pandey, R. Rai, M. Pal and S. Pandey, *Phys. Chem. Chem. Phys*, 2014, **16**, 1559–1568.

7 S. Zahn, B. Kirchner and D. Mollenhauser, *Chem. Phys. Chem.*, 2016, **17**, 3354–3358.

8 B. D. Ribeiro, C. Florindo, L. C. Iff, A. Z. Coelho and I. M. Marrucho, *ACS Sustain. Chem. Eng.*, 2015, **3**, 2469–2477.

9 D. J. G. P. van Osch, L. F. Zubeir, A. van der Bruinhorst, M. A. A. Rocha and M. C. Kroon, *Green Chem.*, 2015, **17**, 4518–4521.

10 A. Sanchez-Fernandez, T. Arnold, A. J. Jackson, S. L. Fussell, R. K. Heenan, R. A. Campbell and K. J. Edler, *Phys. Chem. Chem. Phys*, 2016, **18**, 33240–33249.

11 T. Arnold, A. J. Jackson, A. Sanchez-Fernandez, D. Magnone, A. E. Terry and K. J. Edler, *Langmuir*, 2015, **31**, 12894–12902.

12 L. Sapir, C. B. Stanley and D. Harries, *J. Phys. Chem. A*, 2016, **120**, 3253–3259.

13 R. Esquembre, J. Sanz, J. G. Wall, F. del Monte, C. R. Mateo and M. L. Ferrer, *Phys. Chem. Chem. Phys*, 2013, **15**, 11248–11256.

14 J. T. Gorke, F. Srienc and R. J. Kazlauskas, *Ionic Liquid Applications: Pharmaceuticals, Therapeutics, and Biotechnology*, American Chemical Society, 2010, vol. 1038, ch. 14, pp. 169–180.

15 J. T. Gorke, F. Srienc and R. J. Kazlauskas, *Chem. Commun.*, 2008, **0**, 1235–1237.

16 H. Monhemi, M. R. Housaindokht, A. A. Moosavi-Movahedi and M. R. Bozorgmehr, *Phys. Chem. Chem. Phys*, 2014, **16**, 14882–14893.

17 B.-P. Wu, Q. Wen, H. Xu and Z. Yang, *J. Mol. Catal. B: Enzym.*, 2014, **101**, 101–107.

18 A. R. Harifi-Mood, R. Ghobadi and A. Divsalar, *Int. J. Biol. Macromol.*, 2017, **95**, 115–120.

19 F. Milano, L. Giotta, M. R. Guascito, A. Agostiano, S. Sblendorio, L. Valli, F. M. Perna, L. Cicco, M. Trotta and V. Capriati, *ACS Sustain. Chem. Eng.*, 2017, **5**, 7768–7776.

20 A. Sanchez-Fernandez, K. J. Edler, T. Arnold, D. Alba Venero and A. J. Jackson, *Phys. Chem. Chem. Phys.*, 2017, **19**, 8667–8670.

21 F. Merza, A. Fawzy, I. AlNashef, S. Al-Zuhair and H. Taher, *Energy Reports*, 2018, **4**, 77–83.

22 S. Bryant, R. Atkin and G. G. Warr, *Langmuir*, 2017, **33**, 6878–6884.

23 S. Bryant, R. Atkin and G. G. Warr, *Soft Matter*, 2016, **12**, 1645–1648.

24 M. C. Gutiérrez, M. L. Ferrer, C. R. Mateo and F. del Monte, *Langmuir*, 2009, **25**, 5509–5515.

25 H. Mohwald, *Annu. Rev. Phys. Chem.*, 1990, **41**, 441–476.

26 S. Kewalramani, H. Hlaing, B. M. Ocko, I. Kuzmenko and M. Fukuto, *J. Phys. Chem. Lett.*, 2010, **1**, 489–495.

27 G. van Rossum, *Python tutorial, Technical Report CS-R9526*, Centrum voor wiskunde en informatica (cwi) technical report, 1995.

28 T. Kluyver, B. Ragan-Kelley, F. Pérez, B. Granger, M. Bussonnier, J. Frederic, K. Kelley, J. Hamrick, J. Grout, S. Corlay, P. Ivanov, D. Avila, S. Abdalla and C. Willing, Positioning and Power in Academic Publishing: Players, Agents and Agendas, 2016, pp. 87–90.

29 A. Nelson, S. Prescott, I. Gresham and A. R. McCluskey, *refnx v0.0.17*, 2018, `http://doi.org/10.5281/zenodo.1327191`.

30 A. Nelson, *Journal of Applied Crystallography*, 2006, **39**, 273–276.

31 Y. Gerelli, *Journal of Applied Crystallography*, 2016, **49**, 330–339.

32 M. Björck and G. Andersson, *Journal of Applied Crystallography*, 2007, **40**, 1174–1178.

33 J. Goodman and J. Weare, *Comm. App. Math. Comp. Sci.*, 2010, **5**, 65–80.

34 D. Foreman-Mackey, D. W. Hogg, D. Lang and J. Goodman, *Publ. Astron. Soc. Pac.*, 2013, **125**, 306.

35 N. Kučerka, M. A. Kiselev and P. Balgavý, *Eur. Biophys. J.*, 2004, **33**, 328–334.

36 P. Balgavý, N. Kučerka, V. I. Gordeliy and V. G. Cherezov, *Acta Phys. Solvaca*, 2001, **51**, 53–68.

37 R. S. Armen, O. D. Uitto and S. E. Feller, *Biophys. J.*, 1998, **75**, 734–744.

38 W. J. Sun, R. M. Suter, M. A. Knewtson, C. R. Worthington, S. Tristram-Nagle, R. Zhang and J. F. Nagle, *Phys. Rev. E*, 1994, **49**, 4665–4676.

39 J. Pan, F. A. Heberle, S. Tristram-Nagle, M. Szymanski, M. Koepfinger, J. Katsaras and N. Kučerka, *BBA - Biomembranes*, 2012, **1818**, 2135–2148.

40 N. Kučerka, B. W. Holland, C. G. Gray, B. Tomberli and J. Katsaras, *J. Phys. Chem. B*, 2012, **116**, 232–232.

41 T. Arnold, C. Nicklin, J. Rawle, J. Sutter, T. Bates, B. Nutter, G. McIntyre and M. Burt, *J. Synchrotron Rad.*, 2012, **19**, 408–416.

42 R. A. Campbell, H. P. Wacklin, I. Sutton, R. Cubitt and G. Fragneto, *Eur. Phys J. Plus*, 2011, **126**, 107.

43 T. Bayerl, R. Thomas, J. Penfold, A. Rennie and E. Sackmann, *Biophy. J.*, 1990, **57**, 1095–1098.

44 S. J. Johnson, T. M. Bayerl, W. Weihan, H. Noack, J. Penfold, R. K. Thomas, D. Kanellas, A. R. Rennie and E. Sackmann, *Biophys. J.*, 1991, **60**, 1017–1025.

45 L. A. Clifton, M. Sanders, C. Kinane, T. Arnold, K. J. Edler, C. Neylon, R. J. Green and R. A. Frazier, *Phys. Chem. Chem. Phys.*, 2012, **14**, 13569–13579.

46 C. A. Helm, H. Möhwald, K. K. r and J. Als-Nielsen, *EPL (Europhys. Lett.)*, 1987, **4**, 697.

47 J. Daillant, L. Bosio and J. J. Benattar, *EPL (Europhys. Lett.)*, 1990, **12**, 715.

48 R. A. Campbell, Y. Saaka, Y. Shao, Y. Gerelli, R. Cubitt, E. Nazaruk, D. Matyszewska and M. J. Lawrence, *J. Colloid Interface Sci.*, 2018, **531**, 98–108.

49 A. Sanchez-Fernandez, G. L. Moody, L. C. Murfin, T. Arnold, A. J. Jackson, S. M. King, S. E. Lewis and K. J. Edler, *Soft Matter*, 2018, **14**, 5525–5536.

50 D. Marsh, *Chem. Phys. Lipids*, 2010, **163**, 667 – 677.

51 D. Small, *J. Lipid Res.*, 1984, **25**, 1490–1500.

52 F. Abelès, *J. Phys. Radium*, 1950, **11**, 307–309.

53 L. G. Parratt, *Phys. Rev.*, 1954, **95**, 359–369.

54 A. R. McCluskey, *lipids_at_airdes*, 2018, `http://doi.org/10.5281/zenodo.1327191`.

55 L. Braun, M. Uhlig, R. von Klitzing and R. A. Campbell, *Adv. Colloid Interface Sci*, 2017, **247**, 130–148.

56 C. Tanford, *The Hydrophobic Effect: Formation of Micelles and Biological Membranes*, John Wiley & Sons Ltd., Somerset, NJ, USA, 2nd edn, 1980.

57 C. M. Hollinshead, R. D. Harvey, D. J. Barlow, J. R. P. Webster, A. V. Hughes, A. Weston and M. J. Lawrence, *Langmuir*, 2009, **25**, 4070 – 4077.

58 E. Jones, T. Oliphant, P. Peterson *et al.*, *SciPy: Open source scientific tools for Python*, 2001, `http://www.scipy.org/`.

59 D. Vaknin, K. Kjaer, J. Als-Nielsen and M. Lösche, *Biophys. J.*, 1991, **59**, 1325–1332.

60 R. J. Gillams, C. D. Lorenz and S. E. McLain, *J. Chem. Phys.*, 2016, **144**, 225101.